

Article

Grain Size Evolution and Mechanical Properties of Nb, V–Nb, and Ti–Nb Boron Type S1100QL Steels

Jan Foder^{1,2}, Jaka Burja³ and Grega Klančnik^{1,*} ¹ Research Center Jesenice d.o.o., Cesta Franceta Prešerna 61, SI-4270 Jesenice, Slovenia; jan.foder@rcjesenice.si² Department of Materials and Metallurgy, Faculty of Natural Sciences and Engineering, University of Ljubljana, Aškerčeva cesta 12, SI-1000 Ljubljana, Slovenia³ Institute of Metals and Technology, Lepi pot 11, SI-1000 Ljubljana, Slovenia; jaka.burja@imt.si

* Correspondence: klanclnik.grega@gmail.com

Abstract: Titanium additions are often used for boron factor and primary austenite grain size control in boron high- and ultra-high-strength alloys. Due to the risk of formation of coarse TiN during solidification the addition of titanium is limited in respect to nitrogen. The risk of coarse nitrides working as non-metallic inclusions formed in the last solidification front can degrade fatigue properties and weldability of the final product. In the presented study three microalloying systems with minor additions were tested, two without any titanium addition, to evaluate grain size evolution and mechanical properties with pre-defined as-cast, hot forging, hot rolling, and off-line heat-treatment strategy to meet demands for S1100QL steel. Microstructure evolution from hot-forged to final martensitic microstructure was observed, continuous cooling transformation diagrams of non-deformed austenite were constructed for off-line heat treatment, and the mechanical properties of Nb and V–Nb were compared to Ti–Nb microalloying system with a limited titanium addition. Using the parameters in the laboratory environment all three micro-alloying systems can provide needed mechanical properties, especially the Ti–Nb system can be successfully replaced with V–Nb having the highest response in tensile properties and still obtaining satisfying toughness of 27 J at –40 °C using Charpy V-notch samples.

Keywords: S1100QL; grain size; microalloying; vanadium; niobium; titanium; boron; mechanical properties; microstructure; non-metallic inclusions



Citation: Foder, J.; Burja, J.; Klančnik, G. Grain Size Evolution and Mechanical Properties of Nb, V–Nb, and Ti–Nb Boron Type S1100QL Steels. *Metals* **2021**, *11*, 492. <https://doi.org/10.3390/met11030492>

Academic Editor: Andrey Belyakov

Received: 16 February 2021

Accepted: 12 March 2021

Published: 16 March 2021

Publisher's Note: MDPI stays neutral with regard to jurisdictional claims in published maps and institutional affiliations.



Copyright: © 2021 by the authors. Licensee MDPI, Basel, Switzerland. This article is an open access article distributed under the terms and conditions of the Creative Commons Attribution (CC BY) license (<https://creativecommons.org/licenses/by/4.0/>).

1. Introduction

High yield strength levels above 550 MPa are required when talking about advanced high-strength steels (AHSS). When tensile strengths above 780 MPa are achieved, the term “ultra-high-strength steels” (UHSS) is used. Nowadays, tensile strengths above 1000 MPa are typical for high-strength steels. Non-standardized S1100QL steel belongs to the group of ultra-high-strength fine-grained martensitic steels. It must meet the minimum yield strength of 1100 MPa and Charpy impact toughness of at least 27 J transverse and 30 J longitudinal to the rolling direction at –40 °C. The latter is referred to as standardized steel grades aimed for similar applications [1]. Superior strength and satisfactory toughness enable the use in the most demanding construction projects, heavy lifting industry, mining, and elsewhere. Ultra-high-strength is the result of various strengthening mechanisms like grain refinement, solid-solution strengthening, precipitation strengthening, and deformation substructure formation [2]. However, to achieve the desired strengthening mechanisms, many factors such as alloying and microalloying, primary and secondary steelmaking, casting practice, hot rolling, and final heat treatment process must be controlled [3,4]. One of the most important factors, affecting final microstructure and mechanical properties, is the use of optimal microalloying technology. Microalloying involves a small addition of elements, usually a maximum 0.1 wt %, that form high-temperature carbides, and ni-

trides. The most common microalloying elements are Nb, Ti, and V, which can be used independently or in combination with each other [5].

Titanium forms small and stable TiN that pin the austenite grain boundaries, thus limiting grain boundary mobility during reheating and hot rolling [4,6]. Ti is also used as a N binding agent for B protection, because of its high affinity to N [7]. Ti addition is limited in respect to nitrogen, not only as of the Ti/N ratio but also as the total product of Ti · N, due to the risk of coarse primary TiN formation [8]. In the case of higher total Ti · N product TiN forms non-metallic inclusions in the last solidification front. These coarse non-metallic inclusions do not provide prior austenite grain (PAG) size control, furthermore, they degrade fatigue properties, weldability, and impact toughness of the final product [8–10].

Niobium primarily forms NbC, which is, according to most industrial and laboratory practice, fully dissolved in austenite solid solution during reheating before hot rolling [11]. Nb in solid solution retards the grain boundary migration and recrystallization kinetics via the solute drag effect [12]. Nb is even more effective in form of strain-induced precipitation (SIP) of NbC, which occurs during an adapted hot rolling strategy. NbC precipitates pin dislocations and austenite grain and subgrain boundaries, thus additionally retarding recrystallization [13–16]. In subsequent heat treatment, NbC precipitates remain undissolved, providing additional PAG size control during austenitization [16,17]. Nevertheless, the precipitates can coarsen during reaustenitization, thus diminishing grain size control, as also possible strengthening [4].

Even higher solubility in austenite is typical for vanadium, which primarily forms fine nitrides or carbides that precipitate around the austenite to ferrite transformation temperature, providing precipitation strengthening and inhibiting static recrystallization during final rolling passes [18–22]. Caution needs to be taken during simultaneous Ti and V addition because Ti forms TiN which is more stable than VN or VC, thus Ti and V addition needs to be carefully planned concerning the N content in steel [21]. In the case of simultaneous Ti and Nb addition co-precipitation of niobium-rich particles on existing TiN is also possible [23].

Boron is another important microalloying element, used to increase hardenability. During austenitization before quenching, B should be in austenite solution, so it can segregate to austenite grain boundaries during quenching [24]. Grain boundary segregation of B lowers the austenite grain boundary energy, thus retards the austenite to ferrite transformation. It also suppresses phosphorus enrichment on the austenite grain boundaries, due to preferential occupation of the grain boundary sites by B atoms [25]. If B is in form of borides like BN, it cannot be fully dissolved during austenitization, that is why Ti is commonly used for B protection, to bind the excess nitrogen. Excess Al and a combination of Al and Ti [26], as also a combination of up to 0.1 wt % Al and under 0.03 wt % Nb is used for B protection, latter is also used to prevent coarse TiN formation [27].

In this study, Nb, Nb–V and Nb–Ti microalloying systems were tested for tensile and toughness properties. The aim was to achieve the best combination of mechanical properties with the mentioned microalloying systems. The Nb additions never exceeded 0.015 wt %. Microstructure characterization, with the emphasis on the PAG size and distribution, was performed from hot-forged, hot-rolled to final heat-treated condition. Each microalloying system was evaluated to determine the most promising system which will meet the demands for S1100QL steel.

2. Materials and Methods

Three laboratory heats of S1100QL, using Nb, V–Nb, and Ti–Nb microalloying systems, were produced in a laboratory vacuum induction furnace and cast as 12 kg, 80 × 80 mm ingots. The experimental steel grades were designed on composition limitations in the EN 10025-6 standard [1] using refined master alloys with close to target composition and low P and S content. Slag-free system and protective inert Ar atmosphere in combination with deep vacuum and induction stirring were used to achieve high cleanliness and chemical

homogeneity of the steel melt. The as-cast ingots were soaked at 1150 °C for 2 h and hot-forged into 60 × 60 mm billets. Billets were then reheated at the temperature of 1200 °C for 2 h and hot-rolled into 12 mm thick strips. Reheating temperature and time ensured that Nb was completely in austenite solid solution to maximize the solute drag effect as well as to get sufficient SIP during hot rolling. Hot rolling was performed with predefined 11 continuous passes with subsequent air-cooling. Finish rolling temperature (FRT) was around 880 °C, ensuring strain energy accumulation and austenite pancaking during the last few passes. The rolling setup for all three heats was made to obtain a similar PAG average. Based on the variation of non-recrystallization temperatures (T_{nr}) with target FRT, the final reduction percentage under T_{nr} varies with the chosen microalloying system. The Nb, V–Nb, and Ti–Nb were finished rolled using 49%, 42%, and 58% of final reduction below the T_{nr} . Detailed analysis of laboratory hot rolling, temperature control, and percentage of final reduction of Ti–Nb S1100QL steel can be found in [28]. The last step in the production process was off-line laboratory heat treatment in an electric furnace, using additional type-K thermocouples for temperature control. Heat treatment consisted of re-austenitization at 900 °C and a holding time of 20 min followed by water quenching (Q) and low-temperature tempering (QT) at 200 °C for 1 h. Low-temperature tempering is commonly used for S1100QL and similar steel grades to relieve the internal stresses, as well as to achieve yield strength increment with minor hardness and tensile strength decrease [29].

The refinement of the effective grain size is essential for improving the properties of the as-quenched or quenched and tempered martensite. As the PAG size becomes larger at the highest soaking temperatures before rolling, a way to control the austenite grain growth is by dispersion of finely distributed particles in austenite. For example, by introducing high-temperature stable TiN and/or using Nb or V (in synergy with Mo) for suppressing the recrystallization process. As hot-rolling in the recrystallization region (in the absence of micro-alloying elements and lack of pinning particles) leads to only moderate grain refinement and homogenization [16]. Therefore, the degradation of mechanical properties is expected, because of potential grain growth during hot rolling, and upon re-heating of the as-rolled strip to austenitization temperature before quenching. The alloy design was therefore optimized in a way that some of the finishing passes, as described above, will be done below T_{nr} as the composition is suitable for controlled-rolling (CR) rather than for recrystallization controlled-rolling (RCR). The later would be in the case where the use of micro-alloying elements would be omitted or by using a changed rolling protocol. Additionally, upon reheating of the strip (or the plate) to austenitization temperature, the austenite grain growth is limited due to the low solubility of Nb precipitates due to minor Nb addition in all three heats, see Table 1. Some limited grain size control can also be expected for V-rich precipitates during re-austenitizing, but not at austenitization temperature due to the high solubility of V-rich precipitates in austenite [16]. The control of grain growth during reheating seems to be important, as in industrial practice the achieved heating rates are much lower than in laboratory conditions, and longer times are needed for re-austenitization. The objective of the presented paper was to evaluate the three chosen combinations of microalloying systems using similar deformation and heat treatment protocols to observe microstructure evolution and still obtaining the needed values for S1100QL instead of comparing the benefits of micro-alloying itself, related to micro-alloyed free grade with same basic composition.

The general chemical composition of the hot-rolled strips was determined by optical emission spectroscopy using ARL MA-310 (Si, Mn, Cr, Ni, Mo, Cu, Al, Ti, Nb, V, and B), C and S were determined by the combustion method using LECO CS-600 and N using LECO TC-500.

Samples for metallographic analysis of hot-forged, hot-rolled, and heat-treated (QT) conditions were prepared, following a standard metallographic procedure of grinding, polishing, and etching using 2 vol.% Nital solution. Microstructure and PAG size evolution were performed using a scanning electron microscope with field emission gun (FE-SEM)

Zeiss Supra VP55 and light microscope Zeiss Axio Imager 2. For PAG size evaluation, a semi-automatic approach was used. At least 500 grains were manually evaluated for the PAG size distribution of each sample. Feret's diameter was automatically calculated, using commercial ImageJ software. Typical non-metallic inclusions were investigated, using energy-dispersive X-ray spectroscopy (EDS) on FE-SEM.

Full-thickness longitudinal flat tensile specimens were prepared, and tests were carried out following EN ISO 6892-1:2017 standard [30], using Zwick/Roell Z600 testing machine. Standard Charpy impact toughness V-notch transverse specimens were machined according to EN ISO 148-1:2016 [31]. Charpy impact toughness tests were carried out on 750 J Zwick/Roell PSW750 pendulum machine at $-40\text{ }^{\circ}\text{C}$. Impact toughness testing was conducted using three specimens for Q and QT to calculate the average. Tensile and toughness testing was conducted for Q and QT, to evaluate the effect of low-temperature tempering on the mechanical properties of S1100QL steel.

A continuous cooling transformation (CCT) diagram has been constructed for steel that displayed the highest response in tensile properties with satisfying toughness as the most promising steel grade for further studies. Cylindrical specimens of 10 mm length and 3 mm diameter were machined from a hot-rolled strip. Samples were not homogenized to record transformation temperature scatter typically for industrial environment. Samples were heated with $1\text{ }^{\circ}\text{C/s}$ to $900\text{ }^{\circ}\text{C}$ with holding time of 15 min and cooling with different cooling rates from 0.1 to $100\text{ }^{\circ}\text{C/s}$ down to room temperature, using Linseis L78 R.I.T.A. dilatometer. Dilatometric curves were obtained and samples were metallographically examined to confirm the characteristic temperatures, determined from dilatometric curves.

Thermodynamic prediction, using Thermo-Calc 2021a with TCFE11 database, was conducted. Equilibrium calculations with full composition for Nb, V-Nb, and Ti-Nb steel were made, and a histogram was constructed showing temperature dependence of liquid, austenite, and ferrite phases as well as nitrides, carbides, and carbo-nitrides for three compositions.

3. Results and Discussion

3.1. Chemical Analysis

The chemical composition of three steel strips is presented in Table 1.

Table 1. Chemical composition of the studied S1100QL steels (wt %).

	C	Si	Mn	S *	Cr	Ni	Cu	Mo	Al	Ti	Nb	V	B *	N *	Fe
Nb	0.19	0.24	0.85	30	0.52	1.30	0.38	0.42	0.06	/	0.013	/	11	29	bal.
V-Nb	0.17	0.23	0.88	30	0.51	1.28	0.37	0.40	0.05	/	0.013	0.02	11	46	bal.
Ti-Nb	0.18	0.23	0.87	30	0.52	1.30	0.35	0.41	0.06	0.013	0.014	/	11	31	bal.

* in ppm.

The hardenability of the steel is increased by the addition of C, Mn, Cr, Ni, Mo, and B [32,33]. The role of medium Mo addition is also limiting the grain size by solute drag effect, which also retards recrystallization during high-temperature deformation, especially in combination with Nb, thus caution needs to be taken that full recrystallization is achieved during roughing rolling phase [34]. Ni addition is used to enhance the toughness properties by decreasing the ductile to the brittle transition temperature. In the Ti-Nb steel, B protection is ensured by sufficient Ti plus Al content, whereas the higher Al content is also used for B protection in steels Nb and V-Nb in respect to low N.

Ti addition is over-stoichiometric in respect to N (4.2), however, the total product of Ti and N is kept low, thus limiting the possible impact toughness degradation due to coarse TiN [35]. According to Yan et al. [8], the total product of Ti and N should be lower than the solubility product at solidus temperature (T_{sol}). This is affected by the equation used to calculate the solubility product, as well as by the method used to determine the T_{sol} . If solubility product is calculated with equation proposed by Kunze et al. [36] the start of the precipitation is predicted above T_{sol} also if T_{sol} is increased by excluding B from

the calculations (1471 °C, calculated with Thermo-Calc 2021a, TCFE11), whereas using equation by Inoue et al. [37] predicts precipitation below T_{sol} .

Nb addition is controlled to allow full solubility at reheating before hot rolling. If equations proposed by Klinkenberg et al. [38] for NbC and Irvine et al. [39], for Nb(C, N) are used for steel Ti–Nb, it is predicted that NbC and Nb(C, N) will be in austenite solid solution at 1103 and 1122 °C, respectively. Similar stands for Nb and V–Nb steels with 1101 and 1089 °C for NbC and 1120 and 1107 °C for Nb(C,N) precipitation, respectively.

3.2. Thermodynamic Predictions

For a better understanding of equilibrium precipitation during and after solidification of microalloying products such as nitrides, carbo-nitrides, or carbides important for grain size control, thermodynamic calculations, using Thermo-Calc 2021a with the newest database TCFE11, was used. Thermodynamic calculations were done with full composition for Nb, V–Nb, and Ti–Nb steel for identifying possible equilibrium stability of liquid phase, austenite, ferrite, borides, TiN, Nb(C,N), and VC (Figure 1).

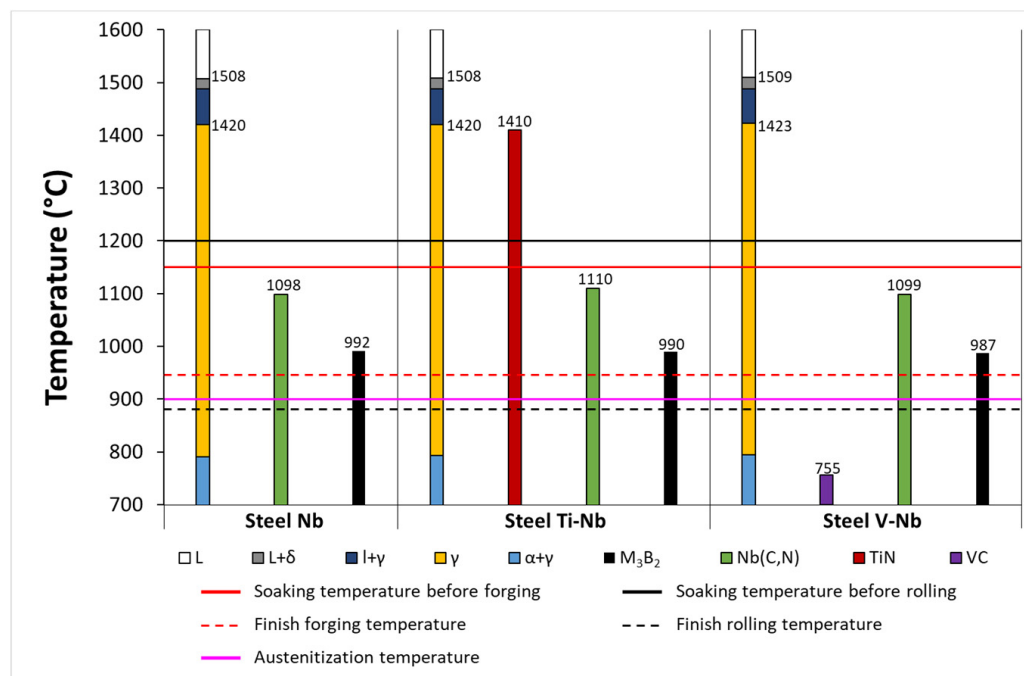


Figure 1. Equilibrium calculations of stability of liquid phase, austenite, ferrite, M_3B_2 , Nb(C,N), TiN, and VC for all three samples. Temperature regions for hot forging, hot rolling, and austenitization are presented.

In the case of Ti–Nb, TiN is predicted to precipitate in solid austenite below T_{sol} which eliminates the possibility of coarse primary TiN formation obeying the Lever rule. The temperature stability of TiN covers the entire austenite region for reheating, multi-pass hot forging, rolling, and cooling, providing the potential for efficient Zener pinning force for austenite grain size control.

The start of the homogeneous precipitation of Nb(C,N) is predicted at 1098, 1099, and 1110 °C for Nb, V–Nb, and Ti–Nb respectively, which ensures full solubility at typical reheating temperatures of around 1200 °C. The temperature of homogeneous precipitation of Nb(C,N) is increased with increasing C content, regardless of the steel grade, which is in accordance with the solubility product of Nb, C, and N [39].

Much higher solubility in austenite is typical for V in V–Nb steel, where V is also dissolved in NbC, since V, Nb, and Ti carbides and nitrides show mutual solubility. Most of the V however remains in austenite solid solution until the beginning of the MC type carbide precipitation at 755 °C, much lower than FRT and chosen re-austenitization temper-

ature for all steels. This means that VC was not present in the austenite during rolling with possible VC precipitation occurring under FRT [22] and dissolving at chosen austenitization temperature.

Precipitation of M_3B_2 (Mo_2FeB_2) phase is predicted around 990 °C, however no BN, $Fe_{23}(C, B)_6$ or Fe_2B formation is predicted, regardless of the microalloying addition used at austenitization temperatures used in this study. The latter was found to decrease the hardenability. Nb and Mo are added to prevent the precipitation of such borides [40].

3.3. Microstructure

Microstructures of hot-forged, hot-rolled, and QT conditions for steel Nb, V–Nb, and Ti–Nb are presented in Figure 2.

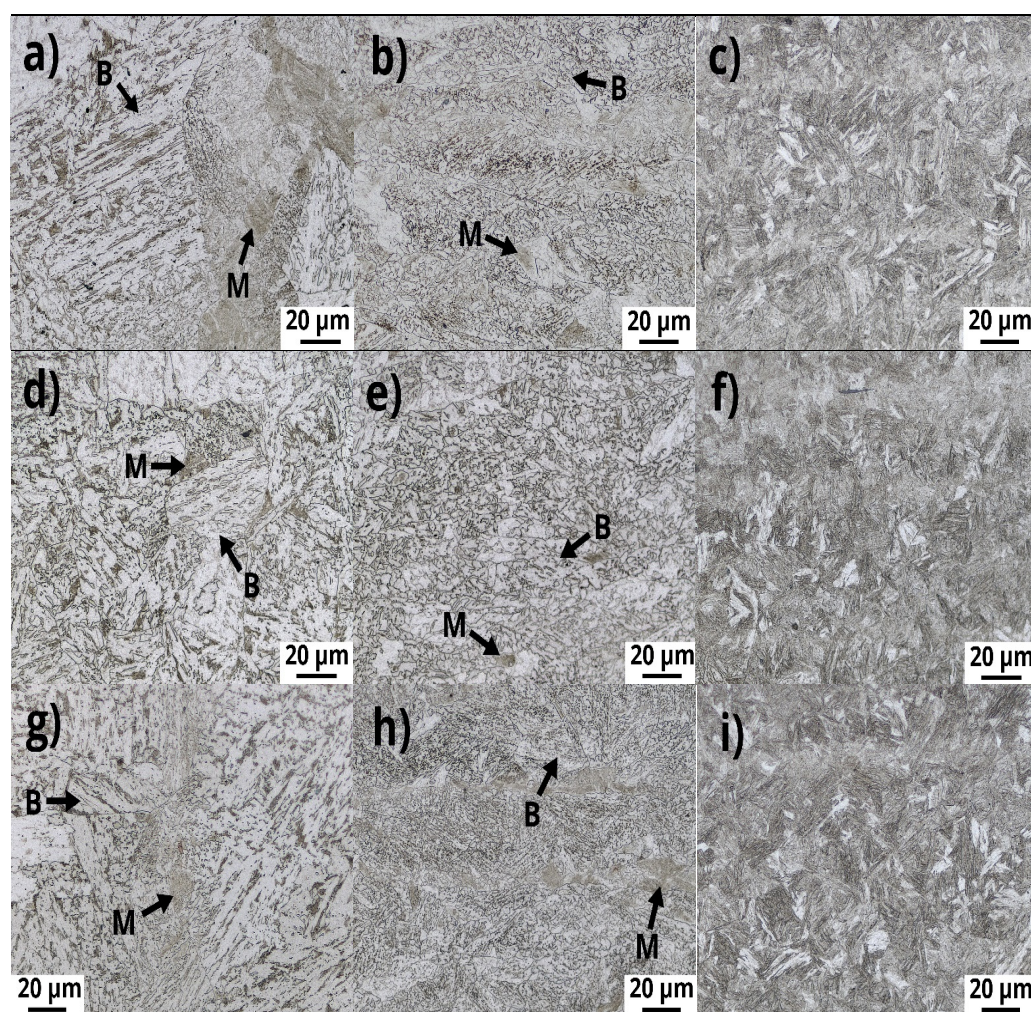


Figure 2. The microstructure of steel Nb, V–Nb, and Ti–Nb for hot-forged, hot-rolled, and low-temperature tempering (QT) conditions. Marks “B” and “M” represent bainite and martensite, respectively. Etched state, light microscopy. (a) Steel Nb, hot-forged; (b) steel Nb, hot-rolled; (c) steel Nb, QT; (d) steel V–Nb, hot-forged; (e) steel V–Nb, hot-rolled; (f) steel V–Nb, QT; (g) steel Ti–Nb, hot-forged; (h) steel Ti–Nb, hot-rolled; (i) steel Ti–Nb, QT.

The microstructures of hot-forged (Figure 2a,d,g) and hot-rolled (Figure 2b,e,h) conditions for all three samples are heterogeneous due to mixed bainitic-martensitic microstructure with predominating bainite. Fractions of martensite are detected in areas of solute enrichment as a part of casting history and recognized as microstructural banding after hot deformation. Microstructural banding as alternating parallel bands is hardly noticeable but still detectable in rolled and QT conditions. The side effect of enrichment of substitutional

alloying elements in the final condition overall negatively influences the impact toughness and weldability response of HSLA steels. At lower cooling rates (air) the alternating bands are usually more pronounced [41].

Coarse equiaxed shaped austenite grains are recognized after a limited absolute reduction during forging (ingot to billet thickness ratio is 1.3) and higher temperature finish (approximately 950 °C) followed by limited cooling of the billets to room temperature (Figure 2a,d,g). The refined mixed microstructure is observed in the hot-rolled state (Figure 2b,e,h) as a part of forged-rolled technology used in this paper with higher final absolute deformation (billet to strip thickness ratio is 5). Because of the finer PAG size and increased cooling rate of a strip with a thinner cross-section and lower measured FRT also the refinement of bainitic ferrite (BF) is visible as a part of bainite (B) in the as-rolled sample. For all steels in the as-rolled condition, prior austenite grains are to some extent elongated (“pancaked”) in a rolling direction, which indicates that some rolling passes of the final reduction are conducted under T_{nr} . More in detail further in this paper, see Figure 6. Theoretic T_{nr} , can be calculated with well accepted [42] equation proposed by Boratto et al. [43], with 921, 899, and 936 °C for steel Nb, V–Nb, and Ti–Nb respectively, which is above measured FRT. It is interesting to notice that even when FRT (approximately 880 °C measured on the rolled surface) is close to predicted T_{nr} for V–Nb the presence of partially elongated grains is evidenced on the defined final reduction of 42%. This is related to the fact that T_{nr} is positioned between recrystallization low temperature (RLT) and recrystallization stop temperature (RST), i.e., temperature where approximately 95 and 5% recrystallization still occurs.

Microstructure after off-line QT heat treatment (Figure 2c,f,i) is fully martensitic (M) and therefore uniform compared to forged and rolled conditions for all three samples, indicating that cooling rate is sufficient for martensite formation and therefore a variation of mechanical properties is not attributed to non-martensitic products. Nevertheless, micrographs reveal some of the unetched white grains as a part of possible untempered martensite achieved after tempering at 200 °C and continuous cooling under air. A closer look reveals a similar fraction of untempered “white” martensite for all steel grades due to similar martensite start (M_s) position (discussed later) and reproducible heat treatment and therefore the variation of toughness values concerning hard and brittle martensite should not be considered as the main cause.

For detailed analysis, a secondary electron (SE) image on FE-SEM was taken for hot-forged, hot-rolled, and QT conditions for steel Ti–Nb. As can be seen from Figure 3a in hot-forged condition microstructure is predominantly bainitic. Bainite is expected since air-cooling was performed after forging. Austenite “pancakes” can be observed after hot rolling (Figure 3b) and much finer bainite plates are formed. The finer microstructure can be expected, since the last rolling passes were done below T_{nr} , introducing a larger number of potential nucleation sites for subsequent bainite nucleation. In QT condition (Figure 3c) microstructure consists of fine lath martensite, which is typical for low-carbon QT steels. Self-tempered martensite (SM) is also observed which is the consequence of a rather high M_s temperature (395 °C and 386 ± 5 , calculated with Thermo-Calc 2021a using database TCFE11 and measured one, respectively). Low-temperature tempering at 200 °C does not alter the martensitic microstructure, however, internal stresses are relieved and some transition ϵ carbides are presumably precipitated [29]. These transition carbides are few nanometers in size and semi-coherent with the matrix, thus cannot be observed using FE-SEM.

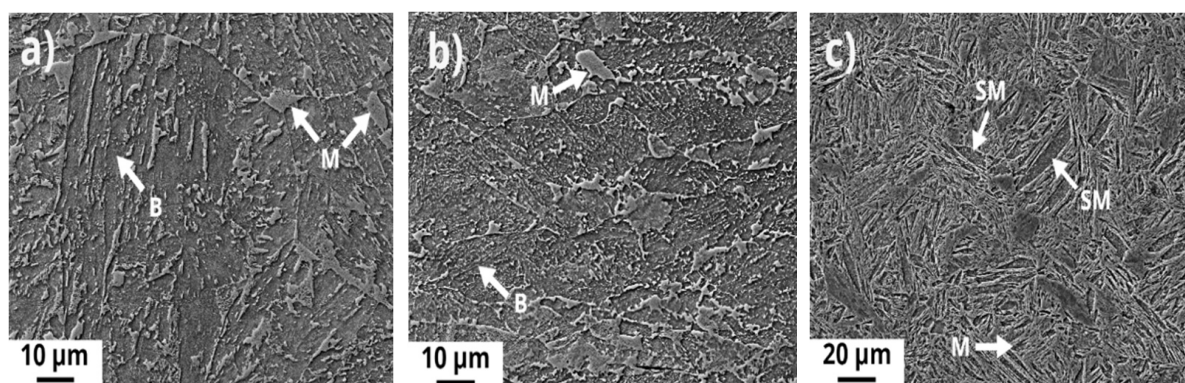


Figure 3. The microstructure of steel Ti–Nb for hot-forged, hot-rolled, and QT conditions. Marks “B”, “M”, and “SM” represent bainite, martensite, and self-tempered martensite, respectively. Etched state, SE image on FE-SEM. (a) Hot-forged; (b) hot-rolled; (c) QT.

3.4. Non-Metallic Inclusions

Typical coarse non-metallic inclusions in hot-rolled conditions are presented in Figure 4.

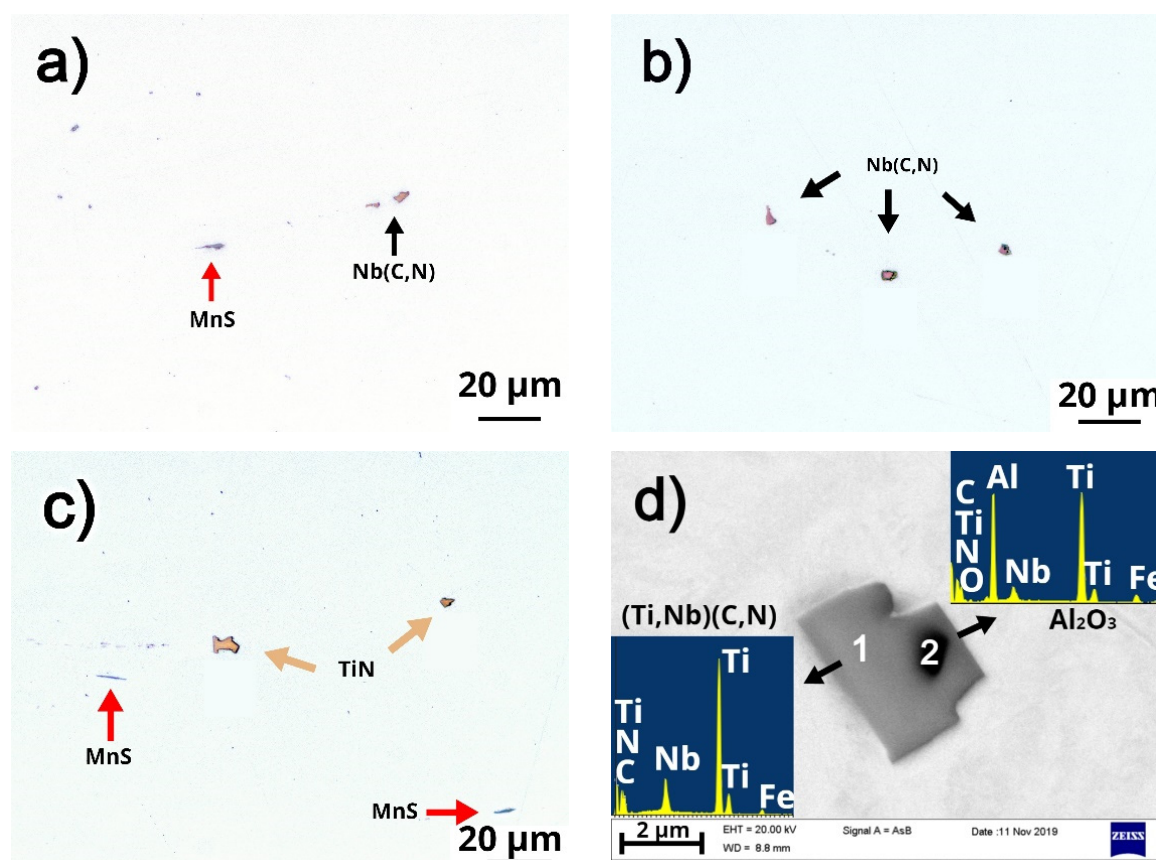


Figure 4. Non-metallic inclusions in steel Nb, V–Nb, and Ti–Nb in hot-rolled conditions. (a) Steel Nb, polished state, light microscopy; (b) steel V–Nb, polished state, light microscopy; (c) steel Ti–Nb, polished state, light microscopy; (d) steel Ti–Nb, FE-SEM BSE image with EDS analysis of the inclusion.

Dark grey non-metallic inclusions in Figure 4a,c (marked by red arrows) represent MnS, which are deformable and oriented in the rolling direction. Black arrows represent primary Nb(C,N) inclusions. They are formed during solidification, because of the solute enrichment, meaning that real solidification follows non-equilibrium solidification with limited diffusion in solid. Primary and therefore coarse Nb(C,N) do not contribute to

dislocation and grain and subgrain boundary pinning. In fact, they have a negative effect of depleting Nb from solution, minimizing Nb solute drag effect, as well as negatively affecting isotropy and ductility. Primary Nb(C,N) cannot be easily dissolved in austenite solid solution during reheating before hot rolling and are taken as non-metallic inclusion working as a stress concentrator. Primary (Ti,Nb)(C,N) and TiN are presented in Figure 4c. Nb(C,N) and (Ti,Nb)(C,N) can be differentiated already on light microscopy by color, since Ti-rich inclusions have orange-golden color, while Nb-rich inclusions have brown-red color. They also differ in shape, since TiN are more cuboidal than Nb(C,N).

Figure 4d shows a backscattered electron (BSE) image with EDS analysis of typical non-metallic inclusion in Ti–Nb micro-alloyed steel. EDS spectrum peaks, marked as 1, correspond to (Ti,Nb)(C,N), which has nucleated on Al_2O_3 (marked as 2). Based on the stability of Nb- and Ti-rich inclusions, TiN has nucleated on Al_2O_3 and later enriched on Nb and C, forming complex primary (Nb,Ti)(C,N) non-metallic inclusion.

No clusters of coarse primary non-metallic inclusions were detected, which occurs in the interdendritic regions, where solute enrichment takes place. These clusters are harmful for final mechanical properties, deteriorating final toughness, and tensile properties thus must be avoided.

Obtained results differ from thermodynamic predictions for TiN and NbC (Figure 1), however, predictions were made for equilibrium conditions, while non-equilibrium conditions are typical for solidification. Solute enrichment of Nb, Ti, C, and N during solidification occurs, exceeding the solubility product and forming coarse primary inclusions. The amount of coarse primary non-metallic inclusions should be as little as possible, thus precautions at chemistry design with minor Nb and Ti addition with proper control of C, N, and minimum superheat before casting and casting itself is needed. Later with emphasis on the primary and secondary cooling regime when continuous (strand) casting is used. Regardless of the type of casting, one of the important parameters is mold geometry and related achieved temperature and concentrations gradients during solidification.

3.5. CCT Diagram

The CCT diagram for steel V–Nb is presented in Figure 5a. The variation of nose position for bainite and ferrite plus pearlite as well as M_s and martensite finish (M_f) temperature is marked with the shaded region, related mostly to achieved grain size after rolling. One can assume that the cooling rate after forging was around $1\text{ }^\circ\text{C/s}$, since a very-small fraction of pearlite was present in the microstructure. The cooling rate after hot rolling was somewhat higher, as no pearlite was detected, which is reasonable, since the heat dissipation in a hot-rolled strip of 12 mm thickness was higher than in 60 mm thick ingot, as discussed already previously. The cooling rate during water-quenching exceeded $10\text{ }^\circ\text{C/s}$ and was estimated to be on average approximately 35 to $40\text{ }^\circ\text{C/s}$, providing fully martensitic microstructure through-thickness. M_s was measured at $386 \pm 5\text{ }^\circ\text{C}$, which agrees well with the Thermo-Calc prediction of $395\text{ }^\circ\text{C}$.

According to transformation temperatures determined by dilatometry, Figure 5b, specific dilatometric curves of cooling revealed the transformation start of a new phase from austenite (martensite, bainite, and ferrite, respectively). This is also supported by the measured hardness. Both, dilatometric curves and metallographic characterization were considered, especially for low cooling rates as in [44]. At the lowest cooling rates under $1.5\text{ }^\circ\text{C/s}$, the transformation start for ferrite (F) is recorded but not for the pearlite (P). However, having natural banded microstructure as a part of solidification history, carbide agglomerates formed inside the F. Therefore, the high-temperature region was classified as F + P rather than F, as the latter was never the case. Figure 5b represents three primary dilatometric curves for the highest, intermediate, and lowest cooling rate.

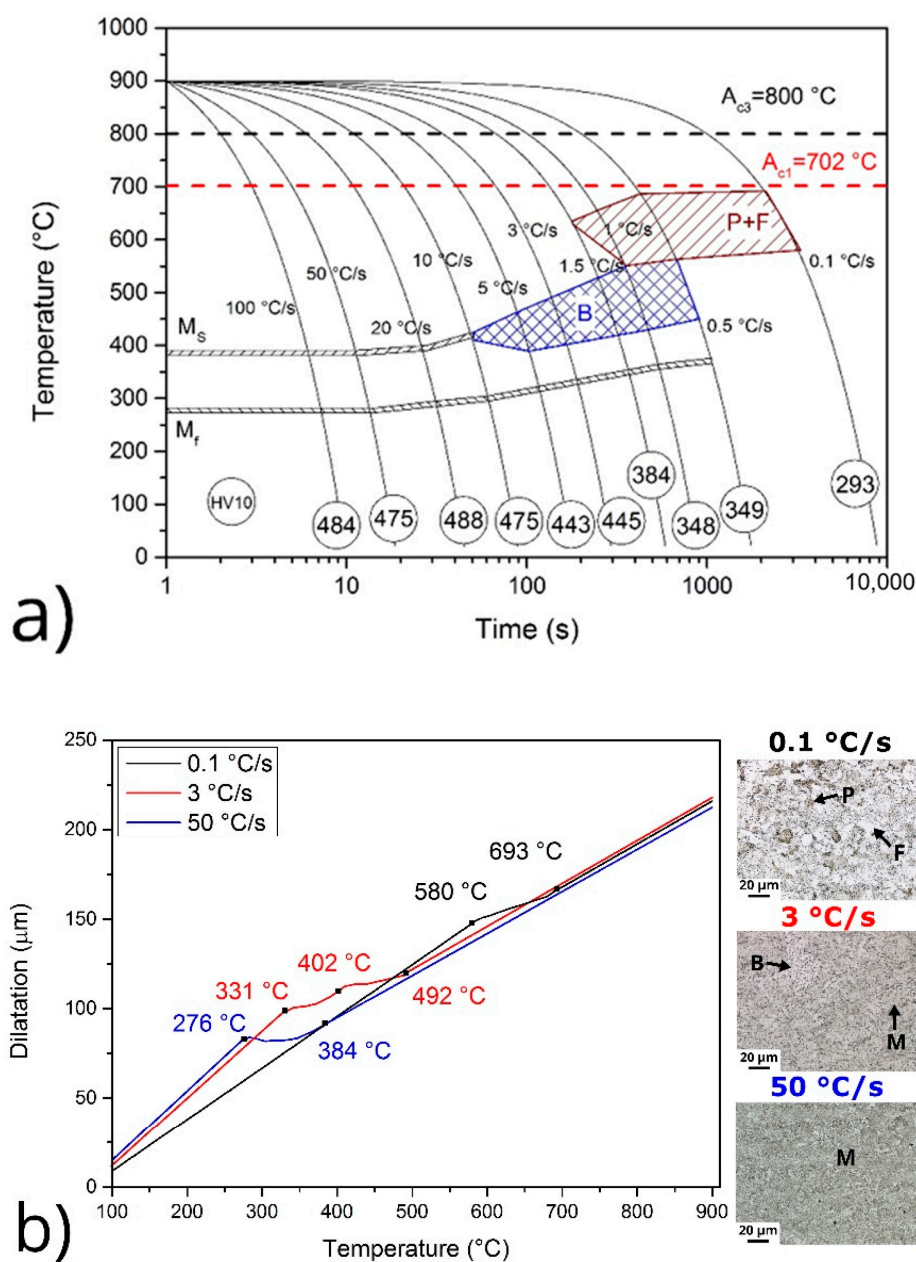


Figure 5. (a) Continuous cooling transformation diagram for steel V–Nb with HV10 hardness measurement for each cooling rate. The shaded region presents the possible variation of Nb and Ti–Nb steel. (b) Dilatometric curves for cooling rates 0.1, 3 and 50 °C/s with representative microstructure. Marks “F”, “P”, “B” and “M” represent ferrite, pearlite, bainite and martensite, respectively.

3.6. PAG Size and Distribution

Another important aspect, affecting final mechanical properties, is PAG size and distribution. Table 2 presents the average and maximum PAG size, standard deviation, and distribution factor G (differencing from grain size number G in terms of ASTM E112) [45]), defined as:

$$G = \frac{d_{\text{avg}}}{d_{\text{max}}}, \quad (1)$$

d_{avg} and d_{max} being average and maximum PAG size in μm , respectively. The higher the value G , the more uniform grain size distribution is expected. Average and maximum PAG size is smallest in Ti–Nb steel regardless of the condition, followed by V–Nb steel, while largest grains were observed in Nb steel. Nevertheless, the difference between all microalloying for average grain size is rather small in the final heat-treated condition.

However, based on the pre-conditioned hot deformation and thermal treatment, these results indicate that Ti has an important role in restricting PAG growth by pinning austenite grain boundaries already in the upper austenite region with the finest maximum achieved grain size. The effect of V is also observed by comparing Nb and V–Nb steel, however, it restricts grain growth to a lesser degree than Ti with constant Nb addition. V effects austenite grain growth by solute drag effect as also by grain and subgrain boundary pinning at lower temperatures. Overall grain refinement was achieved from hot-forged to hot-rolled and subsequent QT conditions for all three samples, indicating the importance of used forging and rolling parameters as a pre-condition for re-austenitization and quenching of S1100QL.

Table 2. Average (d_{avg}) and maximum (d_{max}) grain size, standard deviation (St. dev.) and distribution factor (G) for hot-forged, hot-rolled and QT condition for steel Nb, V–Nb and Ti–Nb.

Steel	Condition	d_{avg} (μm)	d_{max} (μm)	St. dev.	G
Nb	Hot-forged	88.3	585.9	62	0.15
Nb	Hot-rolled	71.1	212.7	31.4	0.33
Nb	QT	18.8	51.1	7.6	0.37
V–Nb	Hot-forged	71	181.5	32.6	0.39
V–Nb	Hot-rolled	58	164.9	29.2	0.35
V–Nb	QT	17.8	48.4	7.3	0.37
Ti–Nb	Hot-forged	58.9	147.2	23.8	0.40
Ti–Nb	Hot-rolled	46.3	150.1	26.9	0.31
Ti–Nb	QT	17.1	42.4	6.1	0.40

Figure 6 shows PAG size distribution for all three steels in hot-forged, hot-rolled, and QT conditions. A total of 500 grains for each condition were measured to obtain statistical distribution. PAG size distribution is significantly narrower in QT condition compared to hot-forged or hot-rolled conditions for all three steels, indicating also the importance of the off-line heat treatment for improving grain size and distribution G and most important the isotropy by forming equiaxed grain structure from the orientated one. However, it needs to be noted that PAG size was calculated as Feret’s diameter, which yields somewhat high values for elongated grains in the case of the rolled condition. Some authors [17] represent effective grain size in the hot-rolled state as the thickness of the austenite “pancakes”.

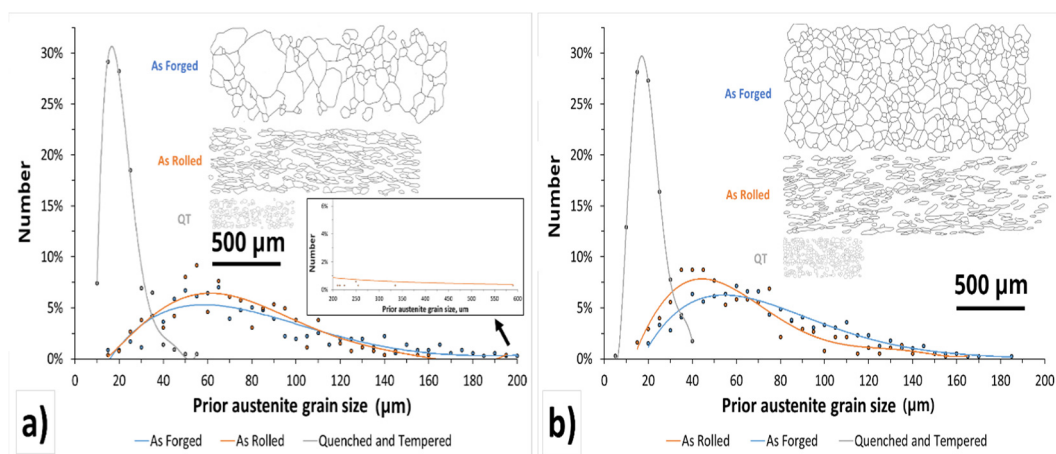


Figure 6. Cont.

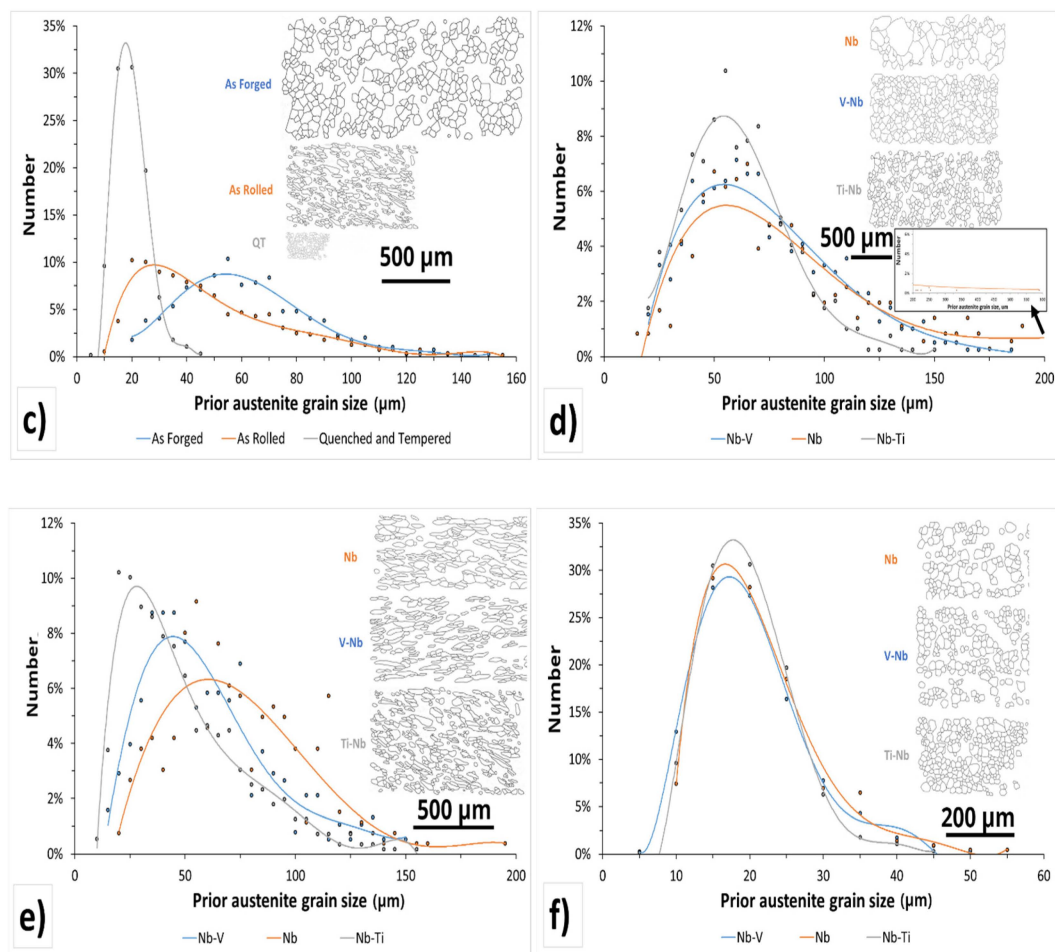


Figure 6. PAG size distribution for Nb, V–Nb, and Ti–Nb steel in hot-forged, hot-rolled, and QT conditions. (a) Nb steel; (b) V–Nb steel; (c) Ti–Nb steel; (d) hot-forged condition; (e) hot-rolled condition; (f) QT condition.

Steel Ti–Nb shows the highest number-percentage of the PAG size in hot-forged, hot-rolled, and QT state, as well as the lowest values of standard deviation (Table 2). Steel Nb on the other side has the largest values of standard deviation, especially in a hot-forged state where extremely large PAG, up to 585 μm , were detected. Differences are less pronounced in the hot-rolled state, however, Nb steel still possesses the widest distribution and peaks at the largest grain size. By careful analysis, no pronounced bimodal distribution was observed and is taken to be mostly unimodal, meaning that in QT condition arithmetical numerical average could be used for trend observation. This is important as we know that in HSLA steels varying degrees of bimodality and their grain size distribution following rolling as also the re-heat condition can exist and have a significant impact on the toughness [46].

3.7. Mechanical Properties

Table 3 and Figure 7 show yield strength ($R_{p0.2}$), tensile strength (R_m), elongation (A_5), and impact toughness at $-40\text{ }^\circ\text{C}$ (KV_2) for Nb, V–Nb, and Ti–Nb steel in Q and QT condition. The highest $R_{p0.2}$ and R_m in QT condition for steel Nb can be contributed to the highest value of carbon equivalent between the three samples. $R_{p0.2}$ for all three samples is increased by low-temperature tempering (200 $^\circ\text{C}$ for 1 h) with a minor decrease in R_m , which is in agreement with other authors [47,48]. The $R_{p0.2}$ increase could be related to the first stage of tempering by precipitation of the fine transition carbides and/or relaxation of internal stresses [29,47,48]. The $R_{p0.2}$ increment for Nb, Ti–Nb, and V–Nb steel is 52, 67, and 112 MPa, respectively, showing that V–Nb steel has the highest potential in terms of tensile properties, also related to the lowest R_m decline after tempering. Obtained results

highlight the importance of low-temperature tempering for tensile properties of S1100QL steel, because all three samples reached the prescribed 1100 MPa $R_{p0.2}$ in QT state, while only Nb steel had more than 1100 MPa $R_{p0.2}$ in the quenched state. The percentage of elongation (A_5) is above the minimum elongation of 10% and does not show any trend when comparing Q and QT conditions.

Table 3. Yield strength ($R_{p0.2}$), tensile strength (R_m), impact toughness at $-40\text{ }^\circ\text{C}$ (KV_2) and elongation (A_5) for steel Nb, V-Nb, and Ti-Nb in Q and QT condition.

Steel	$R_{p0.2}$ (MPa)		R_m (MPa)		KV_2 (J)		A_5 (%)	
	Q	QT	Q	QT	Q	QT	Q	QT
Nb	1144 ± 25	1196 ± 26	1474 ± 30	1395 ± 29	40 ± 0.7	38 ± 0.7	13.0 ± 0.4	11.0 ± 0.3
V-Nb	1074 ± 23	1186 ± 26	1400 ± 29	1384 ± 29	39 ± 1.0	40 ± 0.6	13.0 ± 0.4	12.0 ± 0.4
Ti-Nb	1093 ± 24	1160 ± 25	1426 ± 30	1377 ± 29	43 ± 1.4	45 ± 1.2	12.5 ± 0.4	13.5 ± 0.4

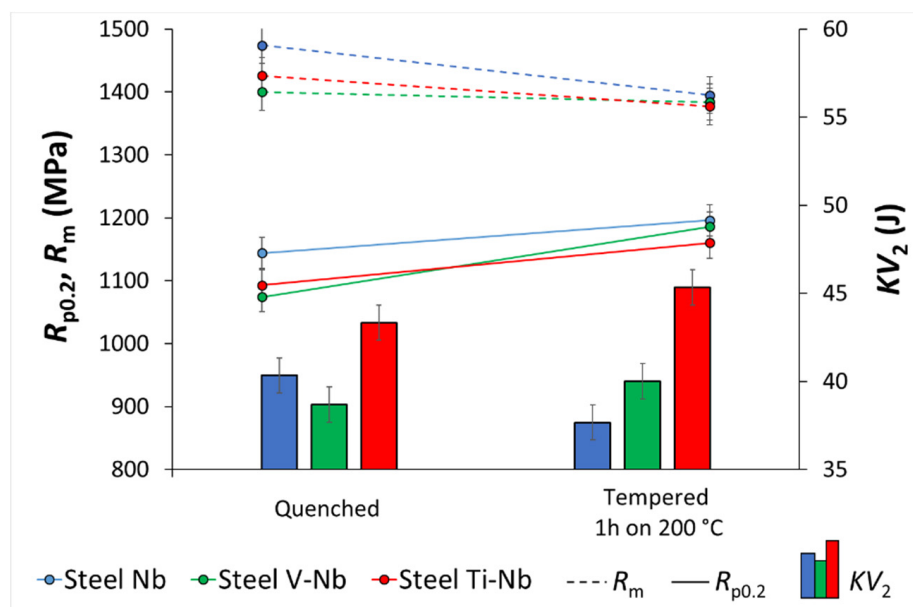


Figure 7. Yield strength ($R_{p0.2}$), tensile strength (R_m), and impact toughness at $-40\text{ }^\circ\text{C}$ (KV_2) for steel Nb, V-Nb, and Ti-Nb in quenched and tempered condition.

Impact toughness exceeds prescribed minimal value of 27 J in Q and in QT condition. Steel Ti-Nb has the highest impact toughness in both Q and in QT condition, which can be correlated to the smallest PAG size and narrowest distribution [34,49] and achieved cleanliness with a low density of coarse-type non-metallic inclusions. Small and homogeneous PAG size in Ti-Nb steel is the consequence of austenite grain growth control by TiN pinning effect during reheating before hot forging and hot rolling, as well as during hot deformation itself. The toughness overall was not improved after low tempering temperature. This could be partly related to high M_s with $395\text{ }^\circ\text{C}$ and modest quenching rate with effective self-tempering during the quenching process. Also, limited presence of hard and brittle as-quench martensite to be additionally tempered to increase the toughness in combination with $R_{p0.2}$ increase with an increased fraction of precipitates as a part of the first stage of tempering of transition carbides [48,50]. The increase of toughness is expected by increasing the tempering temperature; however, it will also result in lower tensile strength levels suitable for S960QL not S1100QL.

4. Conclusions

Microstructure and mechanical properties of Nb, V–Nb, and Ti–Nb boron type S1100QL steels were investigated. Based on the results, the following conclusions can be drawn:

- Microstructures in the hot-forged, hot-rolled, and QT conditions are similar, regardless of the microalloying system used. The microstructures were mostly bainitic after hot forging and hot rolling, followed by air cooling. Fine lath martensite formed after water-quenching.
- Due to microalloying, low-density coarse primary Nb(C,N) and (Ti,Nb)(C,N) non-metallic inclusions formed, however, no V-rich inclusions were observed. No harmful clusters of non-metallic inclusions were detected which resulted in optimal toughness and tensile properties.
- The selection of a microalloying system played a major role in PAG size and distribution. When only Nb was micro-alloyed the resulting PAG size was coarsest, and the widest grain size distribution was obtained. The combination of V–Nb resulted in finer grains and a narrower grain size distribution. However, the combination of Ti–Nb had the smallest PAG size and the narrowest grain size distribution, which is attributed to the pinning effect of TiN.
- Results show that the combination of microalloying elements provides the most favorable mechanical characteristics and grain size distribution compared to the addition of sole microalloying elements, Nb in this paper.
- All three microalloying systems can provide the necessary mechanical properties using appropriate rolling schedules with final reductions done under the T_{nr} resulting in an elongated austenite structure with an increased dislocation density for the nucleation of finely dispersed pinning particles of Nb, V, and Ti, that inhibited the austenite grain growth.
- The V and Nb micro-alloyed steel showed the best response in terms of $R_{p0.2}$ increment at low-temperature tempering at 200 °C, while the Ti–Nb steel achieved the best impact toughness, which correlates well to PAG size and distribution results.

Author Contributions: Conceptualization, G.K.; methodology, G.K. and J.F.; investigation, J.F., G.K., and J.B.; writing—original draft preparation, J.F.; writing—review and editing, G.K. and J.B. All authors have read and agreed to the published version of the manuscript.

Funding: This research is co-financed by the Republic of Slovenia and the European Union from the European Social Fund/European Regional Development Fund/Cohesion Fund, Ga No. C3330-18-952013.

Data Availability Statement: Not applicable.

Acknowledgments: This research was made as a part of ČMRLJ research project co-financed by the Republic of Slovenia and the European Union under the European Regional Development Fund.

Conflicts of Interest: The authors declare no conflict of interest.

References

1. *Hot Rolled Products of Structural Steels—Part 6: Technical Delivery Conditions for Flat Products of High Yield Strength Structural Steels in the Quenched and Tempered Condition*; EN 10025-6 Standard; European Committee for Standardization: Brussels, Belgium, 2019.
2. Kennett, S.C. Strengthening and Toughening Mechanisms in Low-C Microalloyed Martensitic Steel as Influenced by Austenite Conditioning. Ph.D. Thesis, Colorado School of Mines, Golden, CO, USA, 2014.
3. Zhao, J.; Jiang, Z. Thermomechanical processing of advanced high strength steels. *Prog. Mater. Sci.* **2018**, *94*, 174–242. [[CrossRef](#)]
4. Baker, T.N. Titanium microalloyed steels. *Ironmak. Steelmak.* **2018**, *46*, 1–55. [[CrossRef](#)]
5. Baker, T.N. Microalloyed steels. *Ironmak. Steelmak.* **2016**, *43*, 264–307. [[CrossRef](#)]
6. Blancas-Garcia, V. A New View of the Grain-Coarsening Behavior of Austenite in Ti-Microalloyed Low-Carbon Steels. Master's Thesis, University of Pittsburgh, Pittsburgh, PA, USA, 2016.
7. Shen, H.; Hansen, S.S. Effect of the Ti/N ratio on the hardenability and mechanical properties of a QT C-Mn-B steel. *Metall. Mater. Trans. A* **1997**, *28*, 2027–2036. [[CrossRef](#)]
8. Yan, W.; Shan, Y.Y.; Yang, K. Effect of TiN inclusions on the impact toughness of low-carbon microalloyed steels. *Metall. Mater. Trans. A* **2006**, *37*, 2147–2158. [[CrossRef](#)]

9. Burja, J.; Koležnik, M.; Župerl, Š.; Klančnik, G. Nitrogen and nitride non-metallic inclusions in steel. *Mater. Tehnol.* **2019**, *53*, 919–928. [[CrossRef](#)]
10. Zhang, L.P.; Davis, C.L.; Strangwood, M. Dependency of fracture toughness on the inhomogeneity of coarse TiN particle distribution in a low alloy steel. *Metall. Mater. Trans. A* **2001**, *32*, 1147–1155. [[CrossRef](#)]
11. Roy, S.; Karmakar, A.; Mukherjee, S.; Kundu, S.; Srivastava, D.; Chakrabarti, D. Effect of starting microstructure on austenite grain sizes developed after reheating of HSLA steel. *Mater. Sci. Technol.* **2014**, *30*, 1142–1153. [[CrossRef](#)]
12. Suehiro, M. An analysis of the solute drag effect of Nb on recrystallization of ultra low carbon steel. *ISIJ Int.* **1998**, *38*, 547–552. [[CrossRef](#)]
13. Yang, Y.; Zhao, X.M.; Dong, C.Y.; Zhao, X.Y. Influence of hot deformation and precipitates on the recrystallization of Nb-V-Ti free-cutting steel. *Metals* **2020**, *10*, 1587. [[CrossRef](#)]
14. Vervynckt, S.; Verbeken, K.; Thibaux, P.; Liebeherr, M.; Houbaert, Y. Austenite recrystallization-precipitation interaction in niobium microalloyed steels. *ISIJ Int.* **2009**, *49*, 911–920. [[CrossRef](#)]
15. Rešković, S.; Benić, L.S.; Lovrenić-Jugović, M. The interdependence of the degree of precipitation and dislocation density during the thermomechanical treatment of microalloyed niobium steel. *Metals* **2020**, *10*, 294. [[CrossRef](#)]
16. Mohrbacher, H. Property optimization in as-quenched martensitic steel by molybdenum and niobium alloying. *Metals* **2018**, *8*, 234. [[CrossRef](#)]
17. Alogab, K.A.; Matlock, D.K.; Speer, J.G.; Kleebe, H.J. The influence of niobium microalloying on austenite grain coarsening behavior of Ti-modified SAE 8620 steel. *ISIJ Int.* **2007**, *47*, 307–316. [[CrossRef](#)]
18. Quispe, A.; Medina, S.F.; Gomez, M.; Chaves, J.I. Influence of austenite grain size on recrystallization-precipitation interaction in a V-microalloyed steel. *Mater. Sci. Eng. A* **2007**, *447*, 11–18. [[CrossRef](#)]
19. Gomez, M.; Rancel, L.; Medina, S.F. Effects of Nb, V, Ti and Al on recrystallisation/precipitation interaction in microalloyed steels. *Mater. Sci. Forum* **2010**, *638–642*, 3388–3393. [[CrossRef](#)]
20. Wang, P.; Li, Z.; Lin, G.; Zhou, S.; Yang, C.; Yong, Q. Influence of vanadium on the microstructure and mechanical properties of medium-carbon steels for wheels. *Metals* **2018**, *8*, 978. [[CrossRef](#)]
21. Baker, T.N. Processes, microstructure and properties of vanadium microalloyed steels. *Mater. Sci. Technol.* **2009**, *25*, 1083–1107. [[CrossRef](#)]
22. Muckelroy, N.C.; Findley, K.O.; Bodnar, R.I. Microstructure and mechanical properties of direct quenched versus conventional reaustenitized and quenched plate. *J. Mater. Eng. Perform.* **2013**, *22*, 512–522. [[CrossRef](#)]
23. Lechuk, S.J. A Study of Austenite Grain Growth in a Ti-Nb HSLA Steel. Master's Thesis, University of British Columbia, Vancouver, VC, Canada, 1996.
24. Da Rosa, G.; Maugis, P.; Portavoce, A.; Drillet, J.; Valle, N.; Lentzen, E.; Hoummada, K. Grain-boundary segregation of boron in high-strength steel studied by nano-SIMS and atom probe tomography. *Acta Mater.* **2020**, *182*, 226–234. [[CrossRef](#)]
25. Suzuki, S.; Tanino, M.; Waseda, Y. Phosphorus and boron segregation at prior austenite grain boundaries in low-alloyed steel. *ISIJ Int.* **2002**, *42*, 676–678. [[CrossRef](#)]
26. Sharma, M.; Ortlepp, I.; Bleck, W. Boron in heat treatable steels: A review. *Steel Res. Int.* **2019**, *90*, 1900133. [[CrossRef](#)]
27. Hulka, K.; Kern, A.; Schrieffer, U. Application of niobium in quenched and tempered high-strength steels. *Mater. Sci. Forum* **2005**, *500–501*, 519–526. [[CrossRef](#)]
28. Foder, J.; Klančnik, G.; Burja, J.; Kokalj, S.; Bradaškja, B. Mean-flow-stress analysis of laboratory hot rolled S1100QL steel with minor Nb addition. *Mater. Tehnol.* **2020**, *54*, 901–908. [[CrossRef](#)]
29. Krauss, G. Tempering of lath martensite in low and medium carbon steels: Assessment and challenges. *Steel Res. Int.* **2017**, *88*, 1700038. [[CrossRef](#)]
30. *Metallic Materials—Tensile Testing—Part 1: Method of Test at Room Temperature*; EN ISO 6892-1 Standard; European Committee for Standardization: Brussels, Belgium, 2019.
31. *Metallic Materials—Charpy Pendulum Impact Test—Part 1: Test Method*; EN ISO 148-1; European Committee for Standardization: Brussels, Belgium, 2016.
32. Asahi, H. Effects of Mo addition and austenitizing temperature on hardenability of low alloy B-added steels. *ISIJ Int.* **2002**, *42*, 1150–1155. [[CrossRef](#)]
33. Han, F.; Hwang, B.; Suh, D.W.; Wang, Z.; Lee, D.L.; Kim, S.J. Effect of molybdenum and chromium on hardenability of low-carbon boron-added steels. *Met. Mater. Int.* **2008**, *14*, 667–672. [[CrossRef](#)]
34. Zurutuza, I.; Isasti, N.; Detemple, E.; Schwinn, V.; Mohrbacher, H.; Uranga, P. Toughness property control by Nb and Mo additions in high-strength quenched and tempered boron steels. *Metals* **2021**, *11*, 95. [[CrossRef](#)]
35. Du, J.; Strangwood, M.; Davis, C.L. Effect of TiN particles and grain size on the charpy impact transition temperature in steels. *J. Mater. Sci. Technol.* **2012**, *28*, 878–888. [[CrossRef](#)]
36. Kunze, J.; Beyer, B.; Oswald, S.; Gruner, W. Thermodynamic data of the formation of titanium nitride in iron. *Mater. Technol* **1995**, *66*, 161–166. [[CrossRef](#)]
37. Inoue, K.; Ishikawa, N.; Ohnuma, I.; Ohtani, H.; Ishida, K. Calculation of phase equilibria between austenite and (Nb,Ti,V)(C,N) in microalloyed steels. *ISIJ Int.* **2001**, *41*, 175–182. [[CrossRef](#)]
38. Klinkenberg, C.; Hulka, K.; Bleck, W. Niobium carbide precipitation in microalloyed steel. *Steel Res. Int.* **2004**, *75*, 744–752. [[CrossRef](#)]

39. Irvine, K.J.; Pickering, F.B.; Gladman, T. Grain-refined C-Mn steels. *Iron Steel Inst. J.* **1967**, *205*, 161–182.
40. Ishikawa, K.; Nakamura, H.; Homma, R.; Fujioka, M.; Hoshino, M. Effect of molybdenum content on the combined effect of boron and molybdenum on hardenability of low-carbon bprpm added steels. *ISIJ Int.* **2018**, *58*, 551–560. [[CrossRef](#)]
41. Shi, L.; Yan, Z.; Liu, Y.; Yang, X.; Qiao, Z.; Ning, B.; Li, H. Development of ferrite/bainite bands and study of bainite transformation retardation in HSLA steel during continuous cooling. *Met. Mater. Int.* **2014**, *20*, 19–25. [[CrossRef](#)]
42. Homsher, C.N. Determination of the Non-Recrystallization Temperature (T_{nr}) in Multiple Microalloyed Steels. Ph.D. Thesis, Colorado School of Mines, Golden, CO, USA, 2013.
43. Barbosa, R.; Boratto, F.; Yue, S.; Jonas, J.J. The influence of chemical composition on the recrystallisation behavior of microalloyed steels. In Proceedings of the Processing, Microstructure and Properties of HSLA Steels, Tokyo, Japan, 6–10 June 1988; Volume 1, pp. 383–390.
44. Costa, P.S.; Reyes-Valdés, F.A.; Saldaña-Garcés, R.; Delgado-Albavera, E.R.; Salinas-Rodríguez, A. Thermal behaviour of a HSLA steel and the impact in phase transformation: SAW process approach to pipelines. In *Characterization of Metals and Alloys*; Springer International Publishing: Cham, Switzerland, 2017; pp. 85–98.
45. *Standard Test Methods for Determining Average Grain Size*; ASTM E112 Standard; ASTM International: West Conshohocken, PA, USA, 2013.
46. Chakrabarti, D.; Davis, C.; Strangwood, M. Characterisation of bimodal grain structures in HSLA steels. *Mater. Charact.* **2007**, *58*, 423–438. [[CrossRef](#)]
47. Firrao, D.; Matteis, P.; De Sario, A. Exploring the low temperature tempering range of low alloy quenched and tempered steels. *Procedia Struct. Integr.* **2019**, *18*, 703–710. [[CrossRef](#)]
48. Haiko, O.; Kaijalainen, A.; Pallaspuro, S.; Hannula, J.; Porter, D.; Liimatainen, T.; Kömi, J. The effect of tempering on the microstructure and mechanical properties of a novel 0.4C press-hardening steel. *Appl. Sci.* **2019**, *9*, 4231. [[CrossRef](#)]
49. Białobrzeska, B.; Konat, Ł.; Jasiński, R. The influence of austenite grain size on the mechanical properties of low-alloy steel with boron. *Metals* **2017**, *7*, 26. [[CrossRef](#)]
50. Bhadeshia, H.K.D.H.; Honeycombe, R. The Tempering of Martensite. In *Steels: Microstructure and Properties*, 4th ed.; Butterworth-Heinemann: Oxford, UK, 2006; pp. 183–208.